Sliding mode control of an active power filter with photovoltaic maximum power tracking

José Antonio Cortajarena[a,*], Oscar Barambones[b], Patxi Alkorta[a], Jon Cortajarena[c]

[a] Engineering School of Gipuzkoa (Eibar), University of the Basque Country, Otaola 29, 20600 Eibar, Spain
[b] Engineering School of Vitoria, University of the Basque Country, Nieves Cano 12, 01006 Vitoria, Spain
[c] Engineering School of Gipuzkoa, University of the Basque Country, Europa Plaza, 1, 20018 Donostia, Spain

ABSTRACT

Nowadays, the increase in solar energy installations as a source of energy is growing considerably. The connection to the grid of these installations generally injects all the power obtained from the panel as active power, making zero the reactive power. The same power injection system can be used to achieve a unit power factor if the active filter feature is integrated in it. In this paper, an active power filter (APF) that can control both, the MPP (maximum power point) of a photovoltaic system (PV) and the power factor of a nonlinear load connected to the grid using a three phase DC/AC power inverter with new sliding mode controllers is presented. Perturbation–observation (P&O) is the used MPPT algorithm and three Sliding Mode Controllers (SMC) are used to regulate the DC voltage of the PV and the current d and q components of the active filter using the PQ theory. With a SMC, no exact knowledge of the model parameters is required and it offers good behavior against unmodeled dynamics, insensitivity to parameter variations and good rejection of external disturbances. The space vector pulse wide modulation (SVPWM) of 7 and 5 segments is implemented in order to check the efficiency and grid current ripple. Several experimental tests have been carried in different conditions, concluding that the presented system provides an efficient maximum power tracking and a good power filter characteristic.

1. Introduction

The most abundant permanent energy resource on earth is solar energy and its availability in the form of radiation is high in many parts of the world.

The German Advisory Council on Global Change (WBGU) conducted an analysis of energy needs and resources in the future until the 2050s and 2100s. This study highlights the important contribution of solar energy to the long-term global energy needs. This scenario is based on the recognition that it is essential to move energy systems towards sustainability throughout the world. The advancement of technology and research in the development of systems based on photovoltaic panels, more economical and with better characteristics, predicts an increase in installations worldwide in the coming years [1].

The energy generated by photovoltaic panels is mainly dependent on the level of solar radiation that affects the photovoltaic panels and their temperature. Therefore, when variations of these parameters occur, the system must locate the maximum power working point. In order to do this, one of the search techniques for the maximum power point of the photovoltaic panel must be used [2,3].

Most grid-connected photovoltaic system schemes use a two-stage energy conversion topology [4–6]. The first stage is a Boost converter to raise the panel voltage above the grid peak voltage. This converter implements the MPPT algorithm. The objective of the second converter, DC/AC, is to inject the energy supplied by the previous converter into the electrical grid.

An experimental study is presented in A Quantitative Comparison of Central Inverters and String Inverters in Utility-Scale Solar Systems in North America [7].

By using a higher DC voltage level, the DC/DC stage can be eliminated. Some of the benefits of increase the DC/AC input voltage are the components reduction, including overcurrent protection devices, combiners, disconnects, etc.; lower labor costs; less copper in the DC collection system; less expensive inverters (less copper, lower current values for components); and lower total cost per watt. The conclusions are that the central inverter is 1% more efficient than the string inverters solution.

Thus, in accordance with the tendency to increase the inverter's input voltage [8], the series-parallel or centralized topology will be used in the presented application, as shown in Fig. 1.

---

* Corresponding author.
E-mail address: josean.cortajarena@ehu.es (J.A. Cortajarena).

Nomenclature		v_C	inverter capacitor voltage
		v_{PV}	solar panel voltage
α, β	direct and quadrature axes expressed in the stationary reference frame	v_{inv}	DC/AC inverter voltage main harmonic
d, q	direct and quadrature axes expressed in the synchronous rotating reference frame	P	active power
		Q	reactive power
		f_{PWM}	inverter commutation frequency
L_g	grid filter inductance	V_{OC}	PV open circuit voltage
R_g	grid filter resistance	I_{SC}	PV short circuit current
θ_e	grid voltage vector angle	V_{MP}	PV maximum power point voltage
ω_e	grid voltage frequency	I_{MP}	PV maximum power point current
i_g	grid current	P_{MP}	PV maximum power point power
i_{PV}	solar panel current	$d(t)$	SMC uncertainty terms
i_F	inverter output current	$S(t)$	SMC sliding variable
i_{F_MPPT}	inverter output current due to the MPPT	β	SMC switching gain
i_{F_APF}	inverter output current due to the APF	λ	voltage controller SMC constant gain
i_{inv_DC}	DC/AC inverter average input current	K_{SMC}	current controller SMC constant gain
v_g	grid voltage	V	Lyapunov function

The local loads of the photovoltaic system can be especially non-linear, such as the rectifier-filter stages of the power supplies of most household appliances [9]. These loads worsen the power factor by increasing losses in transformers and cables fundamentally and leads to power quality problems that may affect other loads connected at the same point of common coupling [10]. Shunt active power filters have been studied and developed as an effective solution to this problem [11–13].

The control of the MPPT in photovoltaic systems and the active power filter characteristic can be combined in one system. In [14] the inverter DC voltage is fixed for the PV panel but no MPPT is implemented and the current is controlled with hysteresis controllers, changing the switching frequency and therefore the ripple of the current and increasing the complexity of input filters. In [15] the PV MPPT is obtained and the PI are the used current controllers. These controllers have to be adjusted with a high bandwidth in order to track correctly the changing reference and this can make the system unstable. In [16] the MPPT is implemented but the current is regulated with a hysteresis controller with the disadvantage of providing a nonconstant switching frequency and therefore a changing current ripple. In [17] a DC/DC first stage is included before the DC/AC converter reducing the overall efficiency and PI controllers with fast dynamic are used to regulate the

current. In [18] where only presents simulation results, the MPPT is implemented and the used controller is a hysteresis controller. The hysteresis band is modulate as a function of Vdc, the slope of reference current and the filter inductance value. Errors in the parameters produce variation in the hysteresis band and therefore in the switching frequency. In [19] the grid currents are regulated using hysteresis current controllers to generate the inverter gating pulses changing the switching frequency and therefore the ripple of the current.

In this paper, the design, implementation and performance analysis of a three phases active power filter with PV MPPT characteristics is presented. The proposed new control scheme can regulate not only the maximum power of a PV but also the power factor of a nonlinear load could be regulated, usually to a unity power factor. It should be noted that achieving a unity power factor the losses in the electric lines are reduced.

The main hardware feature compared to other systems is the elimination of the voltage boosting stage and thus the Boost converter stage is not necessary, and directly the inverter input voltage is regulated with a sliding mode controller to get from the PV the maximum power. The implemented MPPT algorithm is the perturbation and observe (P&O) and to avoid the measurement of the PV panel current the inverter output power is measured and used in the MPPT algorithm.
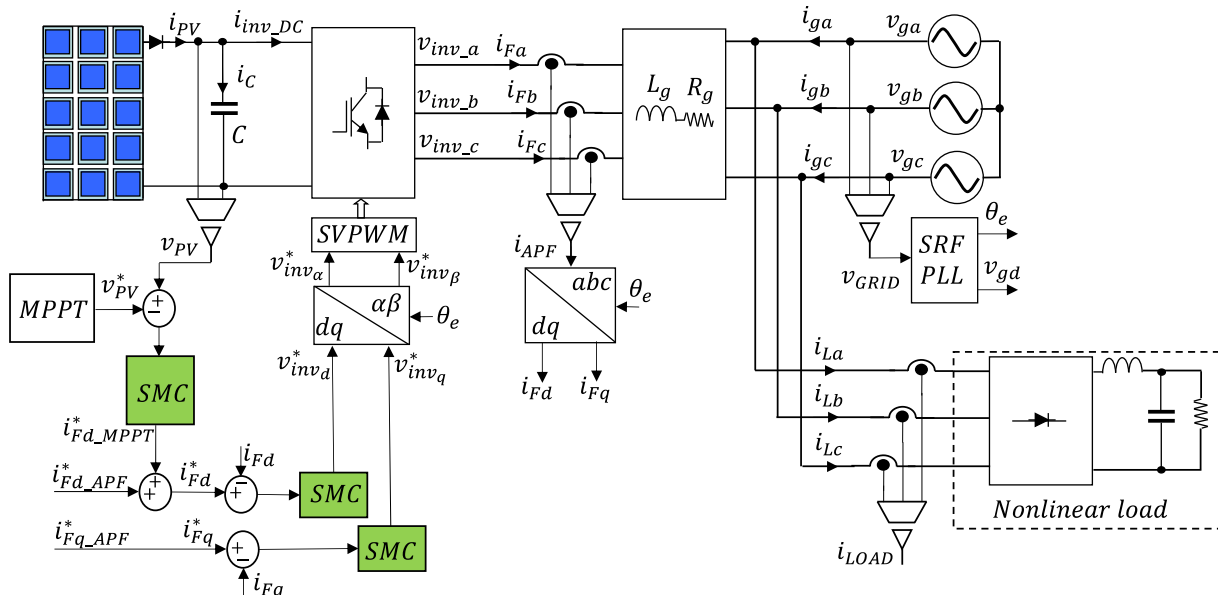

Fig. 1. Active power filter topology, measured signals and SMC controllers.

Some methods of adjustment of conventional controllers such as PI (proportional-integral) or PR (proportional-resonant) require accurate information of the plant model to ensure stability [20]. In this context, the most appropriate option is to consider some type of robust control scheme such as the slide mode control initially developed by Utkin [21] and successfully applied to various types of control structures [22–24]. In [25] a novel terminal sliding mode control method for maximum power tracking of photovoltaic power systems is presented but only for a Boost converter with a resistive load. In [26] a sliding mode control direct power controller based active and reactive power controller for three-phase grid-tied photovoltaic system with a Boost stage is proposed. In [27] a system connected to a PV panel consisting of two cascaded dc–dc boost converters under sliding-mode control are studied in a DC grid. In [28] a novel uncertainty and disturbance estimator based sliding mode control approach is applied to DC–DC power converters and in [29] an adaptive sliding mode control algorithm is developed for grid synchronization of a photovoltaic system.

After the external loop responsible for regulating the panel voltage, two new internal SMC regulators are responsible for regulating the active power filter current by controlling the current d and q components. The proposed current d and q references of the active filter part are generated using the PQ theory.

The stability demonstration of the proposed controllers will be carried out using the Lyapunov stability theory showing that the presented SMC controllers can overcome the system uncertainties, like grid inductance, measurement small errors and noise, and grid voltage tolerances. So, the performance and robustness of the proposed new SMCs is validate in simulation and in a real platform in suitable and adverse conditions. The SMC is also compared experimentally with a conventional PI controller in order to show the performance of the proposed control scheme.

Finally, two space vector pulse wide modulation (SVPWM) techniques are tested, the 7 and 5 segments SVPWM, in order to check the efficiency of the system and the current ripple.

All the experiments are developed on a real platform.

2. System model

The grid to inverter equation that defined the system of Fig. 1 in the stationary reference system is,

$$
\vec{v}_{g\alpha\beta} = \vec{v}_{inv\alpha\beta} - R_g\,\vec{i}_{F\alpha\beta} - L_g\frac{d\vec{i}_{F\alpha\beta}}{dt}
\tag{1}
$$

The system will be controlled in the d-q synchronous rotating reference frame so the equations obtained from (1) are as follows:

$$
v_{gd} = v_{invd} - R_g i_{Fd} - L_g\frac{di_{Fd}}{dt} + \omega_e L_g i_{Fq}
\tag{2}
$$

$$
v_{gq} = v_{invq} - R_g i_{Fq} - L_g\frac{di_{Fq}}{dt} - \omega_e L_g i_{Fd}
\tag{3}
$$

The active and reactive powers are determined in the stationary reference system as,

$$
P = \frac{3}{2}(v_\alpha i_\alpha + v_\beta i_\beta)\,\text{and}\,Q = \frac{3}{2}(v_\beta i_\alpha - v_\alpha i_\beta)
\tag{4}
$$

2.1. Inverter DC voltage control

The MPPT algorithm adjusts the inverter DC voltage according to the perturbation and observe method. However, the MPP voltage level must be higher than the minimum inverter DC voltage required to maintain the regulation, that is, the inverter input voltage should be higher than the grid peak voltage plus the voltage drop in the inductances. If the PV panel is unable to reach this voltage level due to reduced irradiance or increased temperature, the active power filter

will get the energy from the grid to keep the voltage level to the fixed minimum, working in this way as a conventional active power filter. This will be demonstrated in the section on experimental results.

Making a power balance after considering the DC/AC inverter and the filter inductance as ideal and the rotating reference frame linked to the grid voltage ($v_{gq} = 0$), the inverter capacitor current is expressed as,

$$
C\frac{dv_c}{dt} = i_{PV} - \frac{3v_{gd}i_{Fd\_MPPT}}{2v_c}
\tag{5}
$$

From Eq. (5) it is obtained:

$$
\frac{dv_c}{dt} = \frac{1}{C}i_{PV} - g(t)i_{Fd\_MPPT},\ g(t) = \frac{3v_{gd}}{2Cv_c}
\tag{6}
$$

where v_{gd} is the grid voltage peak value and is theoretically constant. Eq. (6) can be rewritten after considering system uncertainties as:

$$
\frac{dv_c}{dt} = \frac{1}{C}i_{PV} - g(t)i_{Fd\_MPPT} + d(t)
\tag{7}
$$

where the term $d(t)$ represents the system uncertainties, like capacitor tolerances, measurement small errors, and grid voltage tolerances.

Let us define the voltage tracking error as follows:

$$
e(t) = v_c - v_c^*
\tag{8}
$$

Taking the derivative of the previous equation with respect to time yields:

$$
\dot{e}(t) = \dot{v}_c - \dot{v}_c^* = \frac{1}{C}i_{PV} - g(t)i_{Fd\_MPPT} + d(t)
\tag{9}
$$

Where it is considered that the reference voltage is a quasi-constant signal because with the MPPT algorithm the change is slow for the control period.

To compensate the system uncertainties an SMC scheme is proposed with the sliding variable $S(t)$ defined as:

$$
S(t) = e(t) + \int_0^t \lambda e(\tau)d\tau
\tag{10}
$$

Then, the sliding surface is defined as:

$$
S(t) = e(t) + \int_0^t \lambda e(\tau)d\tau = 0
\tag{11}
$$

The sliding surface (11) is selected with an integral term in order to avoid the time derivative of the error signal because this derivative will increase the noise signal ratio in a real implementation.

Finally, the sliding mode voltage controller is designed as:

$$
i_{Fd\_MPPT}^*(t) = \frac{1}{g}\left(\lambda e(t) + \beta sgn(S(t)) + \frac{i_{PV}(t)}{C}\right)
\tag{12}
$$

The proposed control signal (12) presents three terms and in order to obtain a good tracking of the voltage trajectory, the gain λ must be chose strictly positive and the switching gain β must be chose $\beta \geq |d(t)|$ for all time. The stability demonstration of the proposed controller is carried out using the Lyapunov stability theory and can be found in [30].

2.2. Inverter active power filter control

The instantaneous reactive power (IRP) p–q theory is the used algorithm to generate the current reference signals in the control of the inverter as active power filter. This algorithm, under the condition that the load is supplied with a sinusoidal symmetrical voltage, shows that the reference signals generation with the IRP p–q theory algorithm provides correct results and the instantaneous values of active and reactive power are [31],

$$
\begin{pmatrix} P_L \\ Q_L \end{pmatrix} = \begin{pmatrix} \bar{P}_L + P_L \\ \bar{Q}_L + Q_L \end{pmatrix}
\tag{13}
$$

$\bar{P}_L$ is the average part of the active power absorbed by the load and must be supplied by the grid and/or by the PV panels. $\bar{Q}_L$ is the average part of the reactive power absorbed by the load and must be supplied by the active power filter in order to get a unity power factor in the grid. P_L and Q_L are the alternating component of the active and reactive powers respectively to be supplied by the active power filter.

Using (4) and taking in consideration the current sense of the inverter, the inverter current components references related with the load instantaneous active and reactive powers are obtained as,

$$\begin{pmatrix} i^*_{F\alpha\_APF} \\ i^*_{F\beta\_APF} \end{pmatrix} = \frac{2}{3\,|v_g|^2}\begin{pmatrix} v_{g\alpha} & -v_{g\beta} \\ v_{g\beta} & v_{g\alpha} \end{pmatrix}\begin{pmatrix} P_L \\ Q_L \end{pmatrix}$$

(14)

With the Park transformation the references in the rotating synchronous reference system are determined,

$$\begin{pmatrix} i^*_{Fd\_APF} \\ i^*_{Fq\_APF} \end{pmatrix} = \begin{pmatrix} cos\theta_e & sin\theta_e \\ -sin\theta_e & cos\theta_e \end{pmatrix}\begin{pmatrix} i^*_{F\alpha\_APF} \\ i^*_{F\beta\_APF} \end{pmatrix}$$

(15)

2.3. Current SMCs

The components of the reference current are therefore,

$$i^*_{Fd}(t) = i^*_{Fd\_MPPT}(t) + i^*_{Fd\_APF}(t)$$

(16)

$$i^*_{Fq}(t) = i^*_{Fq\_APF}(t)$$

(17)

Once the current references are obtained, the controllers to regulate the current d and q components will be designed. Sliding Mode Controllers are used to track the reference current correctly and provide robustness when the real parameters differ slightly from the model and there are system uncertainties.

Considering Eqs. (2) and (3), the derivatives of the components of the current are,

$$\dot{i}_{Fd} = \frac{di_{Fd}}{dt} = -\frac{R_g}{L_g}i_{Fd} + \omega_e i_{Fq} - \frac{v_{gd}}{L_g} + \frac{v_{invd}}{L_g} + d_d(t)$$

(18)

$$\dot{i}_{Fq} = \frac{di_{Fq}}{dt} = -\frac{R_g}{L_g}i_{Fq} - \omega_e i_{Fd} + \frac{v_{invq}}{L_g} + d_q(t)$$

(19)

where the terms $d_d(t)$ and $d_q(t)$ represent the system uncertainties like filter tolerances, measurement small errors, and grid voltage tolerances.

The current components tracking errors are defined as,

$$e_d(t) = i^*_{Fd} - i_{Fd} \quad\text{and}\quad e_q(t) = i^*_{Fq} - i_{Fq}$$

(20)

Taking the derivative of the previous equation with respect to time,

$$\dot{e}_d(t) = \dot{i}^*_{Fd} - \dot{i}_{Fd} = \dot{i}^*_{Fd} + \frac{R_g}{L_g}i_{Fd} - \omega_e i_{Fq} + \frac{v_{gd}}{L_g} - \frac{v_{invd}}{L_g} + d_d(t)$$

(21)

$$\dot{e}_q(t) = \dot{i}^*_{Fq} - \dot{i}_{Fq} = \dot{i}^*_{Fq} + \frac{R_g}{L_g}i_{Fq} + \omega_e i_{Fd} - \frac{v_{invq}}{L_g} + d_q(t)$$

(22)

To compensate the system uncertainties the proposed SMC scheme with the sliding variable $S_d(t)$ and $S_q(t)$ are,

$$S_d(t) = e_d(t) + \int_0^t \left(K_{SMC} + \frac{R_g}{L_g}\right)e_d(\tau)d\tau$$

(23)

$$S_q(t) = e_q(t) + \int_0^t \left(K_{SMC} + \frac{R_g}{L_g}\right)e_q(\tau)d\tau$$

(24)

Finally, the sliding mode current components controllers are designed as:

$$v^*_{invd}(t) = L_g\left(\dot{i}^*_{Fd} + \frac{R_g}{L_g}i^*_{Fd} - \omega_e i^*_{Fq} + \frac{v_{gd}}{L_g} + K_{SMC}e_d(t) + \beta sgn(S_d(t))\right)$$

(25)

$$v^*_{invq}(t) = L_g\left(\dot{i}^*_{Fq} + \frac{R_g}{L_g}i^*_{Fq} + \omega_e i^*_{Fd} + K_{SMC}e_q(t) + \beta sgn(S_q(t))\right)$$

(26)

Now, the stability demonstration of the proposed controller will be carried out using the Lyapunov stability theory. Let us define the following Lyapunov function:

$$V_d(t) = \frac{1}{2}S_d(t)\cdot S_d(t)$$

(27)

Taking the time derivative of the Lyapunov function, and using Eqs. (21), (23) and (25) it is obtained:

$$\begin{aligned} \dot{V}_d(t) &= S_d(t)\cdot\dot{S}_d(t) = S_d(t)\cdot\left(\dot{e}_d(t) + \left(K_{SMC} + \frac{R_g}{L_g}\right)e_d(t)\right) \\ &= S_d(t)\cdot\left(\dot{i}^*_{Fd} + \frac{R_g}{L_g}i_{Fd} - \omega_e i_{Fq} + \frac{v_{gd}}{L_g} - \frac{v_{invd}}{L_g} + d_d(t)\right. \\ &\quad \left. + \left(K_{SMC} + \frac{R_g}{L_g}\right)e_d(t)\right) = S_d(t)\cdot\left(\dot{i}^*_{Fd} + \frac{R_g}{L_g}i_{Fd} - \omega_e i_{Fq} + \frac{v_{gd}}{L_g} - \dot{i}^*_{Fd}\right. \\ &\quad \left. - \frac{R_g}{L_g}i^*_{Fd} + \omega_e i^*_{Fq} - \frac{v_{gd}}{L_g} - K_{SMC}e_d(t) - \beta sgn(S_d(t)) + d_d(t)\right. \\ &\quad \left. + \left(K_{SMC} + \frac{R_g}{L_g}\right)e_d(t)\right) = S_d(t)\cdot(\omega_e e_q(t) + d_d(t) - \beta sgn(S_d(t))) \\ &\leq |S_d(t)|\cdot D_d(t) - \beta\cdot|S_d(t)| \end{aligned}$$

(28)

where $D_d(t)$ is defined as,

$$D_d(t) \geq |\omega_e e_q(t)| + |d_d(t)|$$

(29)

Therefore,

$$\dot{V}_d(t) \leq D_d(t)|S_d(t)| - \beta\,|S_d(t)| \leq 0\,\text{if}\,\beta \geq D_d(t)$$

(30)

Using the Lyapunov's direct method, since $V_d(t)$ is clearly positive-definite, $\dot{V}_d(t)$ is negative definite and $V_d(t)$ tends to infinity as $S_d(t)$ tends to infinity, then the equilibrium at the origin $S_d(t) = 0$ is globally asymptotically stable. Therefore, $S_d(t)$ tends to zero as the time tends to infinity and also $\dot{S}_d(t)$ tens to zero. Moreover, all trajectories starting off the sliding surface $S_d(t) = 0$ must reach it in finite time and then will remain on this surface. So,

$$\dot{S}_d(t) = \dot{e}_d(t) + \left(K_{SMC} + \frac{R_g}{L_g}\right)e_d(t) = 0$$

(31)

Solving the previous equation, it can be concluded that the tracking error $e_d(t)$ converges to zero exponentially.

For the q current component, the same analysis can be done using the next Lyapunov function,

$$V_q(t) = \frac{1}{2}S_q(t)\cdot S_q(t)$$

(32)

3. Active power filter control structure

Fig. 2 shows in a deeper way the structure of the grid-tied three-phase inverter of Fig. 1 working as active power filter with the PV maximum power point tracking characteristic. The main parameters values of the system are shown in Table 1.

A synchronous reference frame phase-locked loop (SRF-PLL) is used for extraction of grid voltage phase, frequency, and amplitude as shown in Fig. 1. The PLL PI controller gains are adjusted as indicated in [32] with a natural frequency of 628 rad/s and a damping factor of 1 [33].

The implemented maximum power point tracking algorithm is the perturbation-observation (P&O). The power for the P&O is calculated using Eq. (4) with the measured grid voltage and the inverter current, avoiding the use of a DC current sensor in the output of the PV array. The grid supplies the load average power and the instantaneous
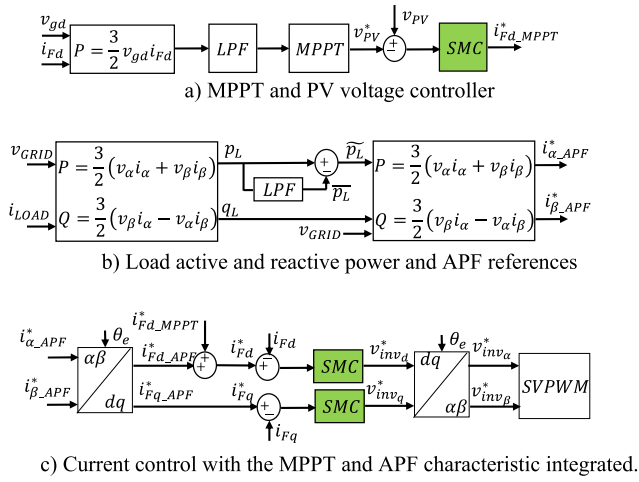
a) MPPT and PV voltage controller

b) Load active and reactive power and APF references

c) Current control with the MPPT and APF characteristic integrated.

Fig. 2. Control structure of the three-phase grid-tied inverter of Fig. 1.

Table 1
Parameters of the system.

Parameter	Value
Grid voltage, v_g	380 V
Grid frequency, $\omega_g = \omega_e$	$2\pi50$ rad/s
Grid filter resistance, R_g	$0.2\,\Omega$
Grid filter inductance, L_g	2 mH
Inverter capacitance, C	$1500\,\mu F$ ($\pm 20\%$)
Inverter modulation frequency, f_{PWM}	20 kHz
PV open circuit voltage, $V_{OC(25\ °C,\ 1000\ W/m^2)}$	670 V
PV sort circuit current, $I_{SC(25\ °C,\ 1000\ W/m^2)}$	4.9 A
PV maximum power point voltage, $V_{MP(25\ °C,\ 1000\ W/m^2)}$	595 V
PV maximum power point current, $I_{MP(25\ °C,\ 1000\ W/m^2)}$	4.4 A
PV maximum power, $P_{MP(25\ °C,\ 1000\ W/m^2)}$	2618 W
Load inductance, L_L	1mH
Load resistance, R_L	$98\,\Omega$
Load capacitance, C_L	$2000\,\mu F$ ($\pm 20\%$)

harmonic power should be supplied by the active power filter. Therefore, the average power should be filtered using a low pass filter. Taking into account that the grid frequency is 50 Hz (and the power harmonics will be even higher), a good cut of frequency for the low pass filter could be 1/5 of the grid frequency. Also the experimental results shown that the used cut off frequency is adequate. The voltage perturbation is a step of 2 V and is realized every 300 ms. The parameters of the SMC inverter DC voltage controller are adjusted taking into account Section 2.1 and its output, $i_{Fd\_MPPT}^*(t)$, is the necessary current component to make the PV work at the maximum power point. However, the MPPT algorithm sets the minimum voltage level, thus operating outside the MPP point, ensuring a voltage level on the DC bus without losing regulation and thus keeping the active filter characteristic working properly.

The active power filter reference is obtained as explained in Section 2.2 and with the calculated $i_{d\_APF}^*$ and $i_{q\_APF}^*$ current references, the inverter total reference is determined as shown in the figure and indicated in Eqs. (16) and (17).

The total d and q current components are regulated using two SMC, generating the inverter d and q voltage references. Both SMCs have been adjusted with the criteria explained in Section 2.3.

The employed PV is an emulated array with the characteristics shown in Table 1. The voltage power characteristic curves of the array for two temperatures and three levels of irradiance are shown in Fig. 3. The shaded area shows the possible operating zone for the inverter. That is, the zone where the inverter input voltage is higher than the grid peak voltage plus the voltage drop in the inductance.

4. Experimental platform

The used experimental test rig is shown in Fig. 4. It is composed of a PC with MatLab/Simulink R2009b (Mathworks, Natick, MA, USA), dsControl 3.7.1 and the DS1006 Controller Board real time interface of dSPACE (dSPACE, Paderborn, Germany), with an AMD Opteron processor to 2.6 GHz. The DC/AC inverter is an INF-50 with an input maximum voltage of 800 V and maximum output current of 25A [34].

The grid voltage is measured using three ISO124 precision isolation amplifiers. The necessary electronic circuit and the interface between the dSPACE and the inverter have also been implemented.

The PV array is emulated with a BK_PVS60085MR and a Magna Power SL80-75 programmable power supplies connected in series with its software for Solar Array Simulation. With this configuration the maximum DC voltage is 680 V.

The 2 mH grid inductance can withstand 12 A to 20 kHz. The SVPWM frequency is fixed to 20 kHz with dead times of 1 µs, establishing a control period of 50 µs. The MPPT algorithm changes the voltage reference every 300 ms for the voltage sliding controller, and because the control period is 50 µs the voltage reference is considered as a quasi-constant value as mentioned in Section 2.1. The β parameter of the SMC should be greater than the system uncertainties. However, as it is well known a bigger β parameter will imply a bigger control activity that is non desirable in practice. After some adjustments and taking in consideration the control activity the adjusted final values are $\beta = 900$ and $\lambda = 30$.

The current sliding controllers are adjusted taking in consideration (29). The $e_q(t)$ term is close to zero when the system is under regulation, therefore the term of more weight is $d_d(t)$. The adjusted values after simulations and in the real platform are $\beta = 7000$ and $K_{SMC} = 3000$.

In the DC/AC inverter, the Space Vector Pulse Width Modulation (SVPWM) switching technique of 7 and 5 segments is implemented. The inverter DC voltage is measured for feedback purposes with the HCNR201 High-Linearity Analog Optocoupler.

The connection of the active filter to the grid is made after guaranteeing with the PLL that the active filter is synchronized with the grid. When this is guaranteed, the filter is connected by means of a contactor and the regulation process begins.

The non-linear load connected to the grid is composed of a three-phase rectifier and a LC filter of 1mH and 2000 µF respectively with a resistive load of 98 Ω. The currents of the non-linear load are measured with three ABB 100P2 BB current sensors to calculate the load active and reactive power.

5. Experimental results

The realized experiments will show first the steady-state behaviour of the system including the Total Harmonic Distortion (THD) of the current when the MPPT is activated and the APF is deactivated or when the MPPT and the APF characteristics are activated. Also the dynamic behaviour when the load is suddenly connected will be shown, the
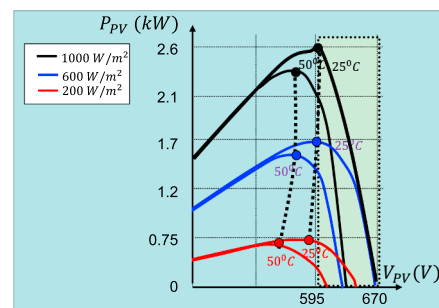

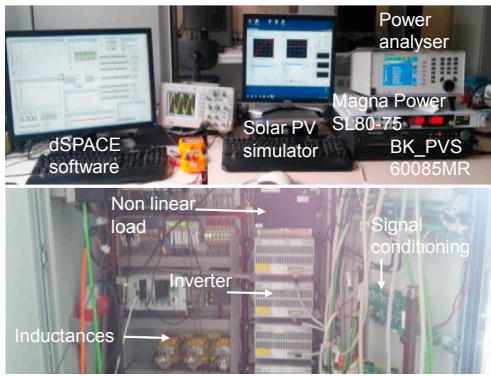**Fig. 3.** Used PV array power characteristic curves.

Fig. 4. Experimental platform.

Fig. 6. Measured grid voltage and current for the case shown in Fig. 5. Grid current harmonics (FFT).

robustness of the system and a comparison with a conventional PI controller will be tested. Finally, the efficiency will be analyzed.

5.1. Steady-state behaviour of the proposed SMCs

Before checking the behaviour of the active power filter, only the characteristic of the MPPT is observed In this sense, Fig. 5 shows the MPP tracking results from the beginning of the system connection. A 0VAR reference of reactive power is imposed to the system. The PV is working with an irradiance of $1000 \, W/m^2$ and a temperature of 25 °C. According to Fig. 3 or Table 1 the expected maximum power is 2618 W.

The P&O MPPT method starts looking for the maximum power point with steps in the voltage reference of 2 V every 300 ms. The voltage sliding controller follows the voltage reference imposed for the MPPT algorithm correctly as can be seen in the figure. The imposed grid current d and q components, i_{gd} and i_{gq}, for the sliding current controllers are also shown in the figure. The measured value follows to the reference perfectly, showing a good adjustment of the sliding current controllers.

As expected, the P&O method produces a ripple due to the MPPT algorithm; even to this ripple, around 2.5%, the maximum power is obtained from the PV. The proof of that can be seen in the MPPT efficiency figure where the obtained efficiency is higher than 99%.

When the MPP point is reached, the minimum efficiency obtained from the PV is 99.1% and the average is 99.7%. The measured grid average power in the steady state zone is 2350 W, slightly lower than the PV maximum power due mainly to the inverter efficiency. In Fig. 6, the grid-side voltage and current are shown when the MPPT algorithm is in steady-state for a unity power factor. The measured power factor is 0.99. The injected current FFT is also shown with a THD in the current of 2.5%.

After checking that the MPPT control is working properly, the behaviour of the active filter is examined with the MPPT characteristic disabled. Fig. 7 shows the grid phase voltage and current for the non-linear load when the active filter is not working. The current total harmonic distortion is 78% and the load absorbed power is 3500 W. When the active filter control is activated the obtained grid phase voltage and current for the nonlinear load are shown in the Fig. 8. The obtained current THD is 4.4%.

5.2. Dynamic behaviour of the proposed SMCs

To observe the dynamic behaviour of the system, a sudden deactivation of the APF will be produced with the MPPT characteristic

Fig. 5. P&O MPP tracking from the initial moment. Irradiance $1000 \, W/m^2$, temperature 25 °C. PV array voltage (V_{PV}), PV current (I_{PV}), MPPT efficiency, grid current d and q components (I_{gd} & I_{gq}) and grid injected active and reactive power (P & Q).
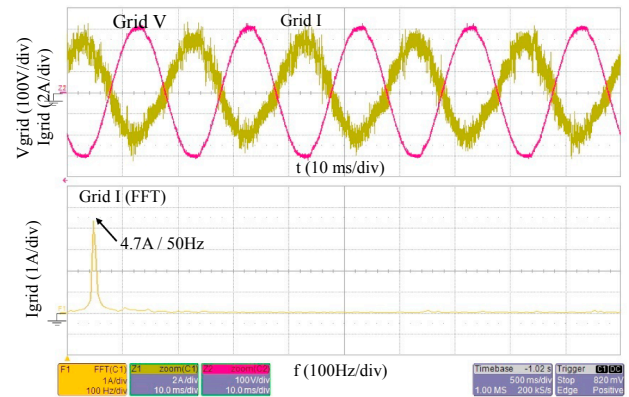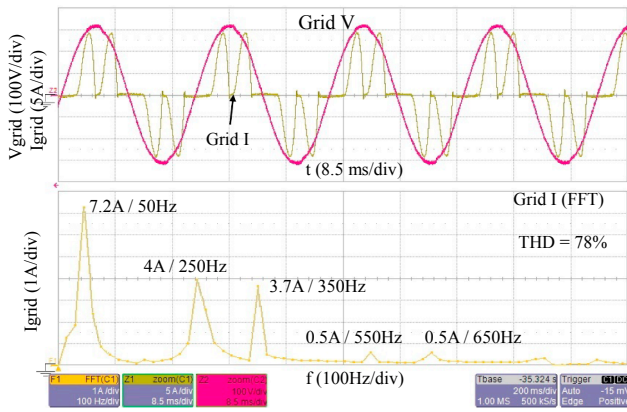
Fig. 7. Grid phase voltage and current when the active filter is disconnected. Grid current harmonics.

Fig. 8. Grid phase voltage and current when the active filter is connected. Grid current harmonics.

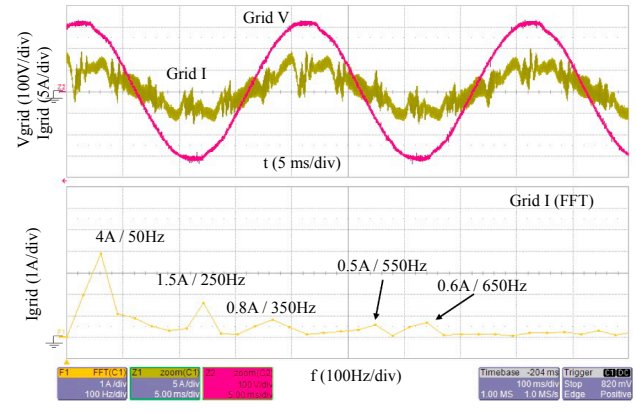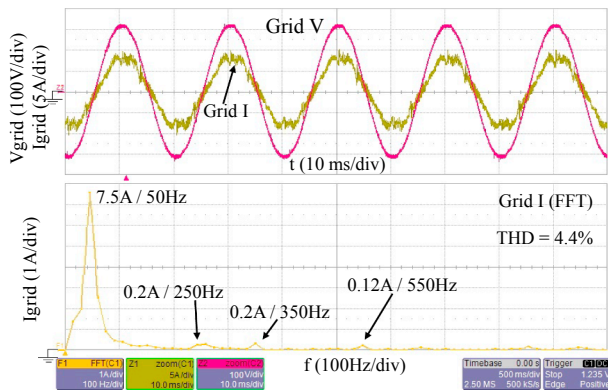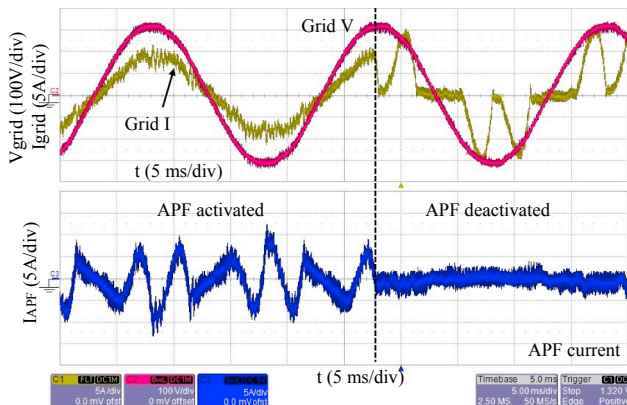**Fig. 9.** Grid phase voltage and current and active power filter current. APF suddenly disconnected.

Fig. 10. Grid phase voltage and current when the APF DC voltage is 580 V.

Fig. 11. Grid phase voltage and current and active power filter current. PV disconnected suddenly.
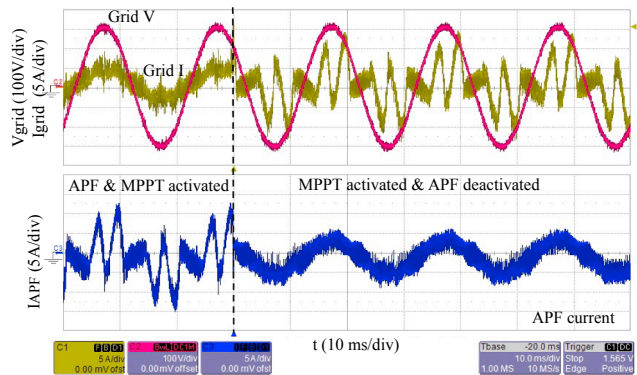
Fig. 12. Grid phase voltage and current and active power filter current. PV working at MPP and APF characteristic disconnected suddenly.

disabled. The determination of the DC bus according to the load current to maintain the control will be determined and tested. The MPPT characteristic will be also suddenly disconnected when the APF characteristic is activated all the time and with the MPPT characteristic activated a sudden disconnection of the APF will also be tested. A sudden disconnection of the load will occur in order to observe the behaviour of the full system. Also, the regulation of the DC bus by the SMC is tested when a step reference is produced.

Fig. 9 shows the behaviour of the active power filter with the MPPT characteristic disabled. The left part of the figure shows the APF characteristic activated and in the right side the APF is suddenly disconnected. Observing the load current and grid voltage, the maximum

load current derivative occurs when the grid voltage is maximum, 15 A/ms. This current derivative has to be created for the active power filter in order to compensate the load current. If Eq. (1) is used disregarding the resistive value, the minimum voltage in the active filter bus DC can be calculated as,

$$V_{C(min)} = \sqrt{3}\left(\widehat{V_g} + L_g \frac{di_F}{dt}\right)$$

(33)

For the values given in Table 1, the minimum active filter bus DC value is 590 V. So, if the MPP value is below this value, the active filter is unable to correct the grid current. This phenomenon can be observed in Fig. 10, where for a DC value of 580 V the grid current distortion is increased considerably. It is therefore necessary to decide whether to
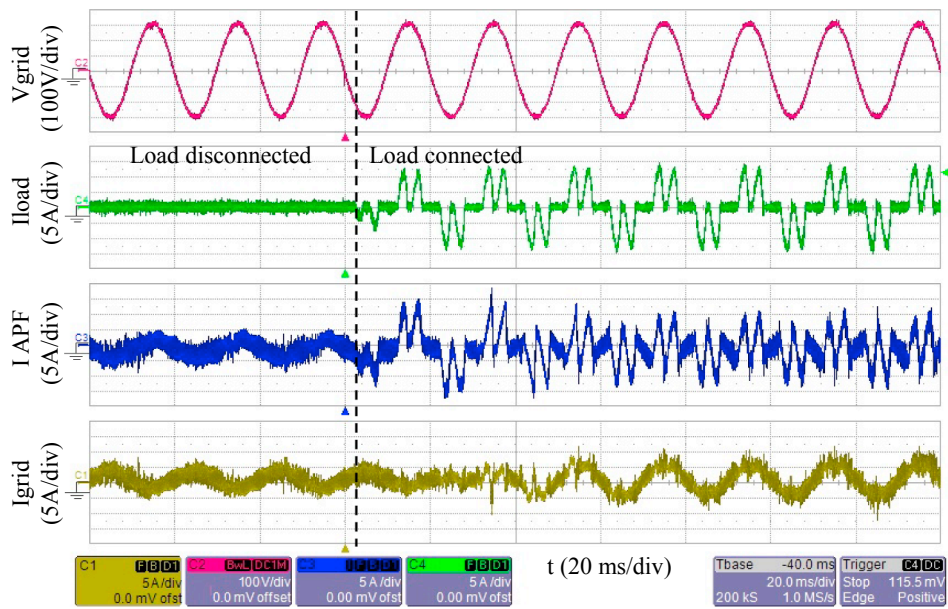
Fig. 13. Grid phase voltage, load current, APF current and grid current. Load suddenly connected.
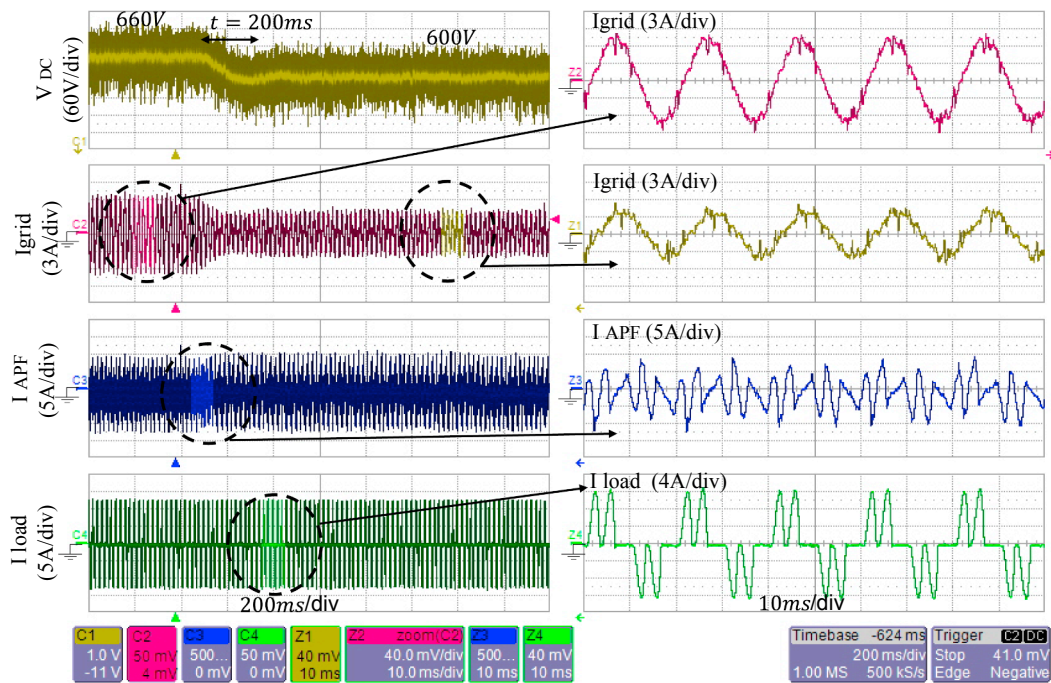

Fig. 14. APF DC voltage, load current, APF current and grid current. DC voltage reference suddenly reduced 60 V.

prioritize the injection of energy into the grid in spite of current degradation or to limit the working point of the photovoltaic panel to ensure that the active power filter corrects the grid current.

It can also be seen in the Fig. 9 that the sum of the grid current and the current generated by the APF results in the load current.

Fig. 11 shows the behaviour of the active power filter and the PV array working at the MPP. The left side of the figure shows a grid current of 1.8 A rms with a supplied power of 1170 W. The rest of the power absorbed by the load is provided by the photovoltaic panel with a value of 2330 W. When the photovoltaic panel is disconnected, all the power absorbed by the load is supplied by the grid as it is shown in the right part of the same figure with a value of 3500 W. All the time the active power filter is correctly compensating the grid current obtaining a unity power factor. Observing the APF current, the left side shows a

higher current due to the injected energy of the PV, however the right side current is only due to the APF effect.

Fig. 12 shows the behaviour of the active power filter with the PV array working at the MPP. The left side of the figure shows a grid current of 1.8A rms with a supplied power of 1170 W. The rest of the power absorbed by the load is provided by the photovoltaic panel with a value of 2330 W. When the active power filter characteristic is disconnected (right side), the grid current is not sinusoidal but 2330 W are supplied for the PV panel and the rest, 1170 W, is absorbed from the grid.

In order to see the dynamic behaviour of the system when there is a sudden load change, the system is extracting energy from the PV panel and the load is disconnected as it is shown in the left part of Fig. 13. In this interval of time the APF is injecting 1400 W into the grid with a
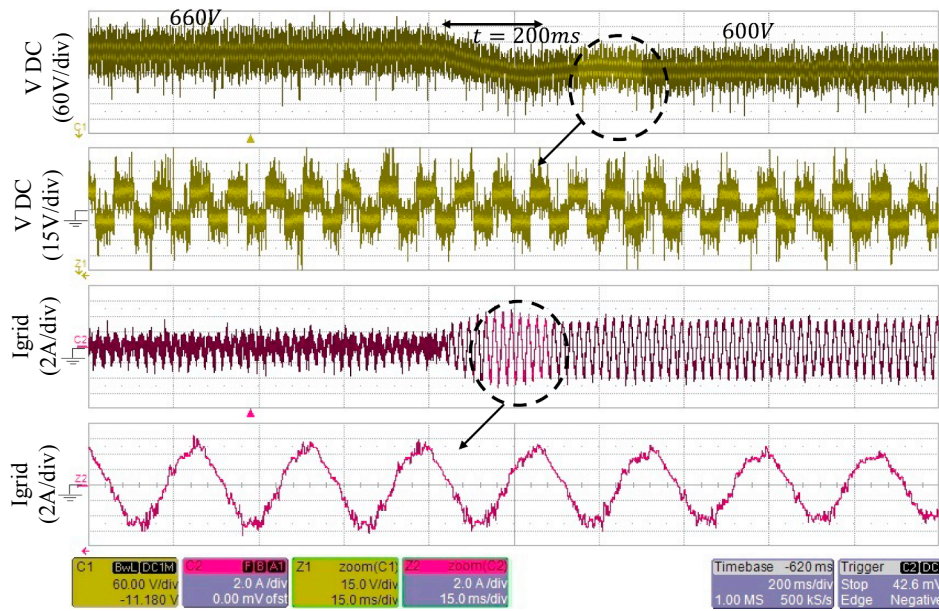
Fig. 15. APF DC voltage and current with noisy in the DC voltage of ± 20 V to 150 Hz. Voltage SMC controller.
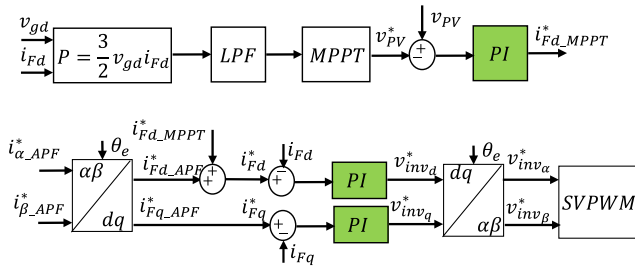

Fig. 16. Control structure with the PI controllers instead of the SMC controllers.

Table 2
Current and voltage SMC and PI comparison.

Parameter	SMC (current)	PI (current)	SMC (voltage)	PI (voltage)
Rise time	1.1 ms	1.2 ms	46 ms	48 ms
Steady state error	0	0	0	0
Settling time	2.1 ms	2.4 ms	152 ms	162 ms
Maximum overshoot	3%	6%	1%	3%

unity power factor. Suddenly the load is connected and the system needs around 60 ms to compensate the grid current as can be seen in the right side of the figure. When the load is connected the power consumed for the load is 3500 W, however due to the injected power of the PV the absorbed power from the grid is 2100 W with unity power factor.

The voltage sliding controller good regulation performance it is shown in Fig. 14. A voltage step reference is produced from an initial value of 660 V to 600 V. At 660 V the PV panel is producing 400 W and due to the system efficiency 350 W are supplied to the load and the rest, 3150 W, are supplied by the grid. When the DC voltage is 600 V, which
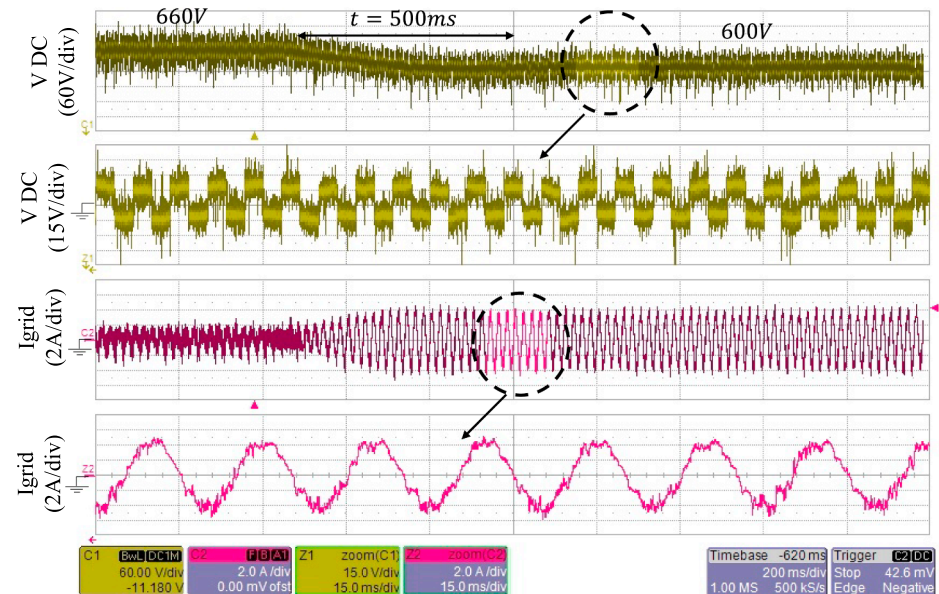

Fig. 17. APF DC voltage and current with noise in the DC voltage of ± 20 V to 150 Hz. Voltage PI controller.
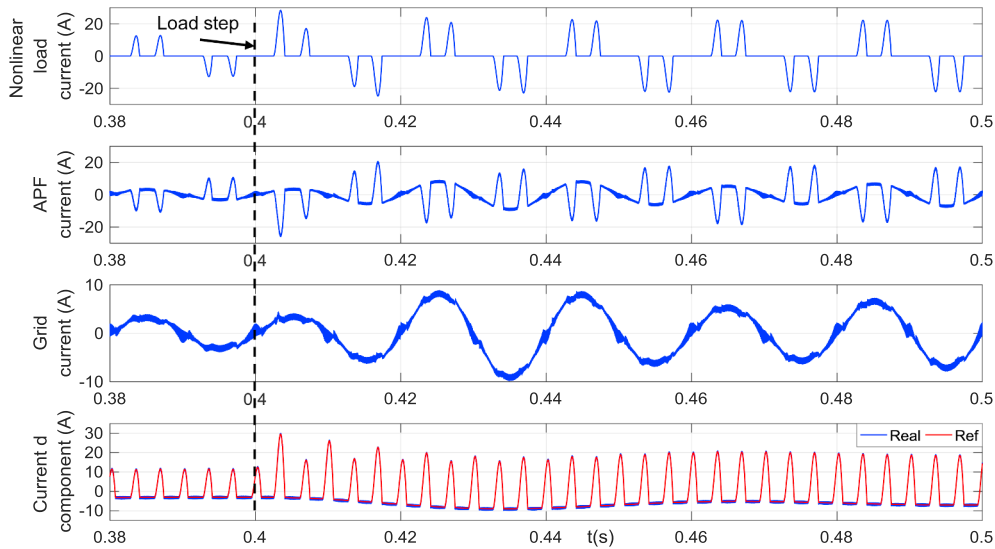
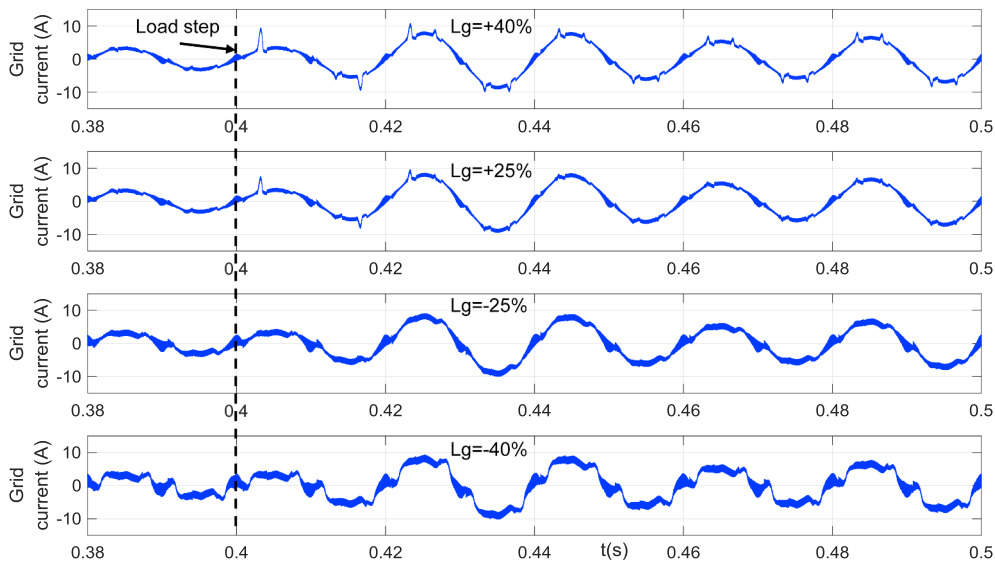**Fig. 18.** Dynamic and static behaviour for a load step in t = 0.4 s when there is not mismatch in Lg and Rg.

Fig. 19. Behaviour for a load step in t = 0.4 s when there is mismatch in Lg. Lg changes from +40% to −40%.
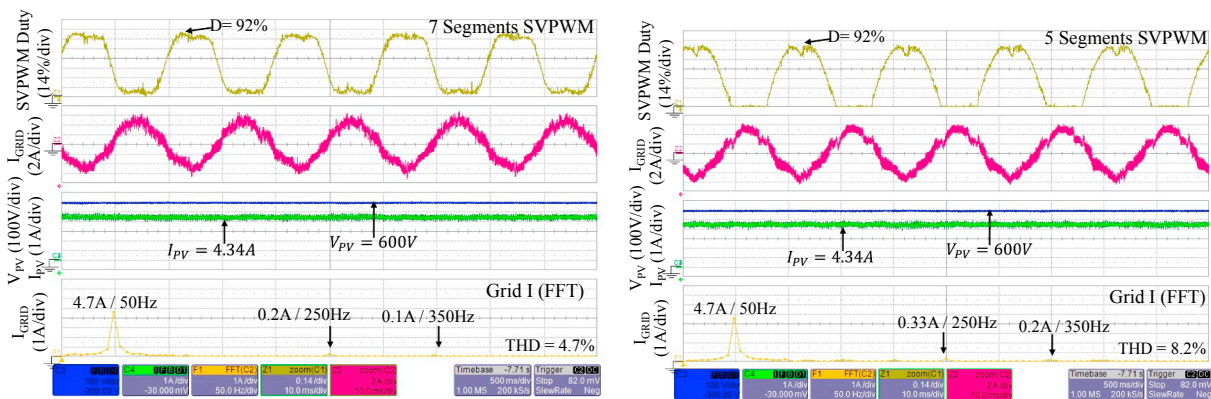

Fig. 20. SVPWM duty cycle, grid current, PV voltage and current and grid current FFT for SVPWM of 7 and 5 segments.

represents 2400 W in the PV panel when the irradiance is 1000 W/m² and the PV temperature is 25 °C due to the efficiency 2130 W are supplied to the load and the grid power is reduced to 1400 W. The time required to reach the reference is 200 ms. This time is fast enough for

the execution of the MPPT algorithm since the variation made in the P& O method every 300 ms is 2 V. The active filter characteristic is well maintained even during the voltage change.

5.3. SMC robustness

As indicated earlier the SMC has the advantage of the disturbance rejection and insensitivity to parameter variations. The *d(t)* term in the controllers includes uncertainties, like grid inductor and resistor tolerances, measurement small errors and noise and grid voltage tolerances among others.

In this sense, Fig. 13 serves to illustrate the good dynamic behaviour of the controlled system when the load is seen as a disturbance. Despite the sudden modification of the load, from no load to a load that consumes 3500 W, the grid current remains sinusoidal.

Also the robustness is tested when noise is originated in the measured PV voltage as it is shown in Fig. 15. A square noise level of ± 20 V and 150 Hz is introduced as can be seen in the zoom. The voltage regulation is good despite the noise when a sudden step from 660 V to 600 V is produced.

There is a slight degradation of the grid current, THD is 9%, but the regulation is good enough despite the noise level, which shows the robust behavior of the slide mode controller. The injected power to the grid when the DC voltage is 600 V is 2200 W.

The control structure with the PI controllers is shown in Fig. 16 where the SMC controllers have been replaced for PI controllers. The PI voltage controller has been tuned experimentally obtaining Kp = 0.2 and Ki = 10. The current PI controllers have been adjusted using Ziegler-Nichols technique, thus the Kp = 0.5 and the Ki = 140. However, due to the noise the PI gains have to be reduced in order to ensure the stability. The result obtained can be seen in Fig. 17, where increases the settling time and the current distortion gets worse, THD is now 11%. Increasing the bandwidth on the PI regulators brings the system closer to instability.

Table 2 shows the summary of the performance characteristics of current and voltage controllers between SMC and PI controllers quantitatively. Based on the data tabulated in Table 2, SMC has the fastest settling time and the lowest overshoot in booth controllers. According to the steady state error, both of the controllers had shown very excellence performance by giving zero error. In term of the rise time, the SMC and the PI controllers have a similar behaviour.

In order to analyze the robustness against Lg and Rg, some simulations are carried out. Fig. 18 shows the behavior for two nonlinear load values when the real value of Lg is used, 2mH. Up to 0.4 s the resistive load RL is 196 Ohm and from that moment the load becomes RL = 98 Ω. The nonlinear load current, the active filter current, the grid current and the d component reference and real current are presented. As expected, the grid current is sinusoidal and the regulation of the d current component with the SMC is very good. However, no mentionable changes in the signals are produced in the simulations when variations on Rg of ± 50% are tested.

When there are variations in the value of Lg, there are also variations in the performance of the system. Therefore, variations in Lg by ± 40% and ± 25% have been simulated. Thus, Fig. 19 shows the current obtained in the grid for different values of Lg. The further away from the nominal value the more degradation the current suffers, however the system remains stable in spite of these variations showing the robustness level of the SMC used.

The spikes observed in the grid current are due to the increased value of Lg and the low value of the DC voltage as indicated in Eq. (33).

5.4. Overall efficiency

Two SVPWM techniques are tested to measure the system efficiency and current THD. Both have the PV panel working to the same power, 2600 W. When the 7 segments SVPWM is the selected modulation, the obtained THD is 4.7% and the measured efficiency is 86% as it is shown in Fig. 20. However, the 5 segments SVPWM improves slightly the efficiency due to lower switching losses, 87.2% but THD gets worse 8.2%. With the 7 segments SVPWM the obtained current THD is lower than the value limited by the IEEE-519 (current THD < 5%) (IEEE Std 519–2014).

The efficiency of the power inverter can be improved by reducing the switching frequency. However, this would result in an increase in the current ripple, worsening the current THD.

6. Conclusions

In this paper, the active power filter feature is added to the inverter used in the PV MPP control. The designed control loops, for the DC bus voltage as well as for the current are made with sliding mode controllers. These controllers were first adjusted by means of several simulations and finally retouched in the real system. The stability of the SMCs is demonstrated using the well-known Lyapunov theory. The used MPPT method is the perturb and observe method with the modification of the power measurement at the AC side of the inverter in order to avoid the use of the DC side current sensor. The active power filter characteristic has been implemented using the PQ theory.

The good static and dynamic behavior of the maximum power point as well as the characteristic of the active filter have been demonstrated experimentally. The robustness of the system against disturbances such as noise in the measurements and grid inductance is also satisfactorily tested. In addition, the system efficiency and current quality are shown for two types of modulation, the seven-segment and five-segment vector modulation. For all these reasons it can be concluded that the presented system provides an efficient maximum power tracking and a good power filter characteristic with the presented sliding mode controllers.

References

[1] www.worldenergy.org/data/resources/resource/solar/; 2013.
[2] Gupta A, Chauhan YK, Pachauri RK. A comparative investigation of maximum power point tracking methods for solar PV system. Sol Energy 2016;136:236–53.
[3] Heslop S, MacGill I. Comparative analysis of the variability of fixed and tracking photovoltaic systems. Sol Energy 2014;107:351–64.
[4] Balato M, Costanzo L, Vitelli M. Reconfiguration of PV modules: a tool to get the best compromise between maximization of the extracted power and minimization of localized heating phenomena. Sol Energy 2016;138:105–18.
[5] Tsai CT, Shen CL, Su JC. A power supply system with ZVS and current-doubler features for hybrid renewable energy conversion. Energies 2013;6(9):4859–78.
[6] Sanseverino ER, Ngoc TN, Cardinale M, Vigni VL, Musso D, Romano P, et al. Dynamic programming and Munkres algorithm for optimal photovoltaic arrays reconfiguration. Sol Energy 2015;122:347–58.
[7] Schneider Electric. A Quantitative Comparison of Central Inverters and String Inverters in Utility-Scale Solar Systems in North America; 2016.
[8] Morgenson J. Director of Business Development, Power Plant Solutions, SMA America. The Commercial Promise of 1,000 VDC PV Design; 2015.
[9] Watson NR, Scott TL, Hirsch S. Implications for distribution networks of high penetration of compact fluorescent lamps. IEEE Trans Power Del 2009;24(3):1521–8.
[10] Montero M, Cadaval E, Gonzalez F. Comparison of control strategies for shunt active power filters in three-phase four-wire systems. IEEE Trans Power Electron 2007;22(1):229–36.
[11] Nikkhah KH, Rafiei S. Optimal control of active power filters using fractional order controllers based on NSGA-II optimization method. Int J Electr Power Energy Syst 2014;63:1008–14.
[12] Yu J, Shiqi D, Yijun W, Weibiao W, Mi D. The engineering design and optimization of main circuit for hybrid active power filter. Int J Electr Power Energy Syst 2013;46:40–8.
[13] Zaveri N, Chudasama A. Control strategies for harmonic mitigation and power factor correction using shunt active filter under various source voltage conditions. Int J Electr Power Energy Syst 2012;42(1):661–71.
[14] Komatsu Y. Application of the extension pq theory to a mains-coupled photovoltaic system. In: Proc. Power Convers. Conf. (PCC), vol. 2. Osaka, Japan; 2002. p. 816–21.
[15] Wu TF, Shen CL, Chang CH, Chiu J. 1φ grid-connection PV power inverter with partial active power filter. IEEE Trans Aerosp Electron Syst 2003;39(2):635–46.

[16] Calleja H, Jimenez H. Performance of a grid connected PV system used as active filter. Energy Convers Manage 2004;45(15–16):2417–28.

[17] Chen X, Fu Q, Yu S, Zhou L. Unified control of photovoltaic grid connection and power quality managements. In: Proc. Workshop Power Electron. Intell. Transp. Syst. (PEITS); Aug. 2008. p. 360–65.

[18] Mosazadeh SY, Fathi SH, Hajizadeh M, Sheykholeslami AR. Adaptive hysteresis band controlled grid connected PV system with active filter function. In: Proc. Int. Conf. Power Eng. Renewable Energy (ICPERE); Jul. 2012. p. 1–6.

[19] Devassy S, Singh B. Design and performance analysis of three-phase solar PV integrated UPQC. IEEE Transactions on Industry Applications, vol. 54. No. 1. January/February 2018. https://doi.org/10.1109/ICPES.2016.7584022.

[20] Vilanova R, Alfaro VM, Arrieta O, Pedret C. Analysis of the claimed robustness for PI/PID robust tuning rules. In: Proc. MED Conf. Control Autom. Marrakech, Morocco; 2010. p. 658–62.

[21] Utkin VI. Sliding mode control design principles and applications to electric drives. IEEE Trans Indus Electro 1993;40(1):26–36.

[22] Barambones O, Garrido AJ. Adaptive sensorless robust control of ac drives based on sliding mode control theory. Int J Robust Nonlin Control 2006;17(9):862–79.

[23] Veselic B, Perunicic-Drazenovic B, Milosavljevic C. High-performance position control of induction motor using discrete-time sliding-mode control. IEEE Trans Ind Electron 2008;55(11):3809–17.

[24] Orłowska-Kowalska T, Kaminski M, Szabat K. Implementation of a sliding-mode controller with an integral function and fuzzy gain value for the electrical drive with an elastic joint. IEEE Trans Ind Electron 2010;57(4):1309–17.

[25] Chian-Song C, Ya-Lun O, Chan-Yu K. Terminal sliding mode control for maximum power point tracking of photovoltaic power generation systems. Sol Energy 2012;86:2986–95.

[26] Ozbay H, Oncu S, Kesler M. SMC-DPC based active and reactive power control of grid-tied three phase inverter for PV systems. Int J Hydrogen Energy 2017;42:17713–22.

[27] Haroun R, El Aroudi A, Cid-Pastor A, Garcia G, Martinez-Salamero L. Impedance matching in photovoltaic systems using cascaded boost converters and sliding-mode control. IEEE Trans Power Electron 2015;30(6):3185–99.

[28] Zhen T, Zijun L, Jingqi Y, Cui W. UDE-based sliding mode control of DC–DC power converters with uncertainties. Control Eng Pract 2019;83:116–28.

[29] Bag A, Subudhi B, Kumar Ray P. An adaptive sliding mode control scheme for grid integration of a PV system. CPSS Trans Power Electron Appl 2018;3(4):362–71.

[30] Cortajarena JA, Barambones O, Alkorta P, De Marcos J. Sliding mode control of grid-tied single-phase inverter in a photovoltaic MPPT application. Sol Energy 2017;155:793–804.

[31] Czarnecki LS. Effect of supply voltage harmonics on IRP-based switching compensator control. IEEE Trans Power Electron 2009;24(2):483–8.

[32] Golestan S, Guerrero JM. Conventional synchronous reference frame phase-locked loop is an adaptive complex filter. IEEE Trans Ind Electron 2015;62(3):1679–82.

[33] Ghartemani MK, Khajehoddin SA, Jain PK, Bakhshai A. Problems of startup and phase jumps in PLL systems. IEEE Trans Power Electron 2012;27(4):1830–8.

[34] Dutt. Power electronics & Control. http://www.duttelectronics.com; 2016.